NANO LETTERS

2008
Vol. 8, No. 6
1654-1659

Highly Efficient Solar Cells using TiO_2 Nanotube Arrays Sensitized with a Donor-Antenna Dye

Karthik Shankar,† Jayasundera Bandara,‡ Maggie Paulose,† Helga Wietasch,‡ Oomman K. Varghese, Gopal K. Mor,† Thomas J. LaTempa,† Mukundan Thelakkat,* and Craig A. Grimes*,†

Department of Electrical Engineering, Materials Research Institute, The Pennsylvania State University, University Park, Pennsylvania 16802, and Applied Functional Polymers, Universitystr-30, University of Bayreuth, 95440 Bayreuth, Germany

Received February 12, 2008; Revised Manuscript Received April 7, 2008

ABSTRACT

Donor antenna dyes provide an exciting route to improving the efficiency of dye sensitized solar cells owing to their high molar extinction coefficients and the effective spatial separation of charges in the charge-separated state, which decelerates the recombination of photogenerated charges. Vertically oriented TiO_2 nanotube arrays provide an optimal material architecture for photoelectrochemical devices because of their large internal surface area, lower recombination losses, and vectorial charge transport along the nanotube axis. In this study, the results obtained by sensitizing TiO_2 nanotube arrays with the donor antenna dye Ru-TPA-NCS are presented. Solar cells fabricated using an antenna dye-sensitized array of 14.4 μm long TiO_2 nanotubes on Ti foil subjected to AM 1.5 one sun illumination in the backside geometry exhibited an overall conversion efficiency of 6.1%. An efficiency of 4.1% was obtained in the frontside illumination geometry using a 1 μm long array of transparent TiO_2 nanotubes subjected to a $TiCl_4$ treatment and then sensitized with the Ru-TPA-NCS dye. Open circuit voltage decay measurements give insight into the recombination behavior in antenna-dye sensitized nanotube photoelectrodes, demonstrating outstanding properties likely due to a reduction in the influence of the surface traps and reduced electron transfer from TiO_2 to ions in solution.

Vertically oriented TiO_2 nanotube arrays fabricated by anodization of titanium are now the focus of research in the fields of catalytic oxidation of organics,[1–4] water photolysis,[5–8] solar energy conversion,[9–11] gas sensing,[12,13] drug delivery,[14,15] and biomedical implants[16] because of several attractive properties related to the unique material architecture of these nanotube (NT) arrays; recent review papers on the topic are available.[17,18] For dye sensitized solar cells, the properties of interest include the large internal surface area, enhanced optical absorption due to scattering effects,[19] and lower recombination. Preliminary studies of ordered one-dimensional architectures including TiO_2 nanotubes and nanowires have indicated that, while the electron transport time is similar to that reported for dye sensitized solar cells made from TiO_2 nanoparticles, the electron recombination time is much larger than for nanoparticulate electrodes resulting in improved charge collection efficiencies.[9,20] In comparison to ordered one-dimensional nanowire electrodes, nanotubes have significantly larger surface area because of the availability of both the internal and the external area of the nanotubes for dye coating.

The donor-antenna dye *cis*-di(thiocyanato)(2,2′-bipyridyl-4,4′-dicarboxylic acid)-(2,2′-bipyridyl-4,4′-bis(vinyltriphenylamine)ruthenium(II) (from here on referred to as Ru-TPA-NCS) contains the electron rich donor triphenylamine linked to the bpy by a conjugated vinyl spacer. The molecular structures of the Ru-TPA-NCS donor-antenna dye and the commercially available N-719 dye (Solaronix, Switzerland) are shown in Figure 1a,b, respectively. The extended π electron delocalization in the bpy ligand that results enables the donor-antenna dye molecules to have high molar extinction coefficients, more than twice that of the commonly used N-719 dye.[21] Furthermore, unlike in N-719, the highest occupied molecular orbitals (HOMO) of Ru-TPA-NCS are spread over the triphenyl amine moieties.[22,23] The increased separation of the HOMO orbitals from the TiO_2 surface has been shown to retard the recombination process at the TiO_2−dye interface and at the TiO_2−hole conductor interface in solid state solar cells.[24] The procedures for the synthesis of the donor-antenna dye have been detailed elsewhere.[24]

In films sensitized by molecular dyes, the thickness of the nanostructured TiO_2 film needs to be at least 10 μm to harvest

* Corresponding author. Email: mukundan.thelakkat@uni-bayreuth.de (M.T.) and cgrimes@engr.psu.edu (C.G.).
† The Pennsylvania State University.
‡ University of Bayreuth.

10.1021/nl080421v CCC: $40.75
Published on Web 04/30/2008

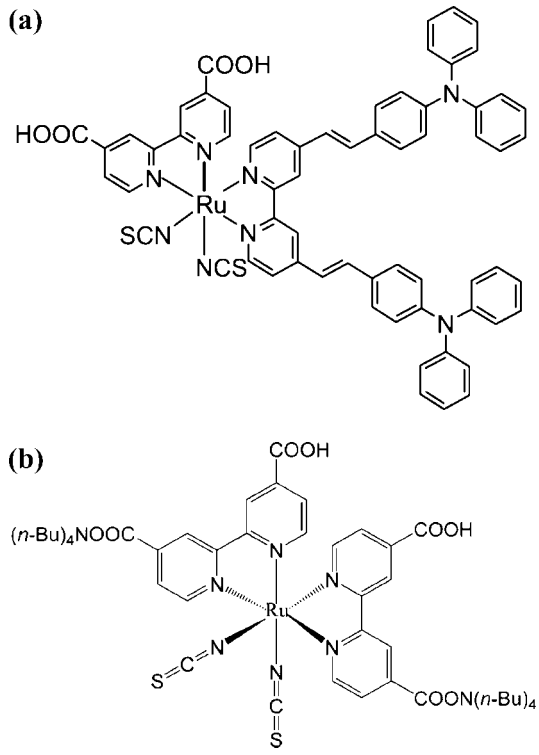

Figure 1. Molecular structure of (a) Ru-TPA-NCS and (b) N-719.

Table 1. Absorption Peaks and Peak Molar Extinction Coefficients of N-719 and Ru-TPA-NCS Dyes Measured in Solution

dye	λ_{max1}	ϵ_1	λ_{max2}	ϵ_2	λ_{max3}	ϵ_3
N-719	309	46400	378	11500	514	11700
Ru-TPA-NCS	307	58300	423	54500	526	24500

the maximal amount of incident photons. By using such a nanocrystalline film of titania sensitized by N-719, a solar-to-electric energy conversion efficiency of 10% has been obtained.[25] The absorption characteristics and molar extinction coefficient of a dye play a crucial role in deciding the performance of a dye-sensitized solar cell. Table 1 gives the absorption peaks and the corresponding molar extinction coefficients of both dyes, Ru-TPA-NCS and N-719. The unprecedented optical density values of Ru-TPA-NCS are the highest reported for (bipyridyl)Ru(II)-dyes, significantly greater that of the N-719 dye. The donor-antenna dye Ru-TPA-NCS exhibits 4−5 times higher molar extinction coefficient than N-719 at 400 nm.[21] Because of the much higher molar extinction coefficient of the Ru-TPA-NCS dye, a much lower film thickness should suffice to harvest a similar amount of incident photons. In this report, we employ vertically oriented TiO_2 nanotube arrays in conjunction with the Ru-TPA-NCS donor-antenna dye to fabricate liquid junction dye sensitized solar cells. The superior molar extinction coefficient of the Ru-TPA-NCS dye manifests itself in the form of much higher light harvesting for electrodes coated with this dye. For example, Figure 2 compares the ultraviolet−visible (UV−vis) absorption spectra obtained from transmittance measurements of 1 μm long transparent TiO_2 nanotube array samples, pristine and coated with Ru-TPA-NCS dye as well as N-719 dye. The nanotube

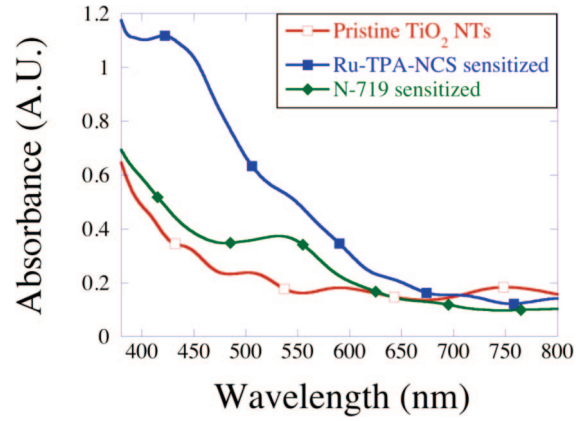

Figure 2. Effect of the dye on optical absorption: (a) Ultraviolet−visible (UV−vis) absorption spectra of pristine 1 μm long transparent TiO_2 Nanotubes (red); Ru-TPA-NCS sensitized 1 μm long transparent TiO_2 nanotubes (blue); and N-719 sensitized 1 μm long transparent TiO_2 nanotubes (green).

samples used for dye coating were nearly identical and in both cases were immersed in dye solution for 24 h. It is clearly evident from Figure 2 that the TiO_2 NT array electrode sensitized with Ru-TPA-NCS dye has higher optical absorption than the N-719 coated sample across the entire solar spectrum with an absorbance more than twice that of the N-719 dye at 470 nm, which corresponds to the wavelength of maximum irradiance in the solar spectrum.

The morphology and active surface area of the vertically oriented TiO_2 nanotubes fabricated by anodization is a function of several variables including the anodization potential and the electrolyte composition.[26–28] The anodization parameters, including electrolyte, influence the relative roughness of the walls of the nanotube morphology. From dye desorption measurements, we have found that the density of active surface sites available for dye adsorption on nanotube electrodes formed in formamide are almost three times that of nanotubes formed in ethylene glycol.[18] To explore the limits of solar cell performance achievable using nontransparent nanotube arrays sensitized with the donor antenna dye, we chose high surface area nanotube arrays formed by anodization for 55 h in formamide-based electrolytes containing 0.14 M NH_4F and 5% deionized water. The resulting nanotubes were 14.4 μm long with an average pore size of 90 nm and a wall thickness of 19 nm. From desorption experiments conducted using N-719 dye, these samples were found to have an effective internal surface area ~1800 times that of a flat unstructured surface.[6] Field emission scanning electron microscope (FESEM) images of the top view and cross section of these nanotube arrays are shown in Figure 3. Crystallinity was induced by annealing the as-anodized samples at 525 °C for 3 h in an oxygen ambient. Further details on TiO_2 nanotube array fabrication have been extensively discussed elsewhere.[26–33]

The $I-V$ characteristics of solar cells fabricated using 14 μm long nontransparent nanotubes sensitized with Ru-TPA-NCS are shown in Figure 4a (assembly and testing details are given in Supporting Information). The cell showed a short circuit photocurrent density (J_{sc}) of 13.44 mA cm^{-2}, an open

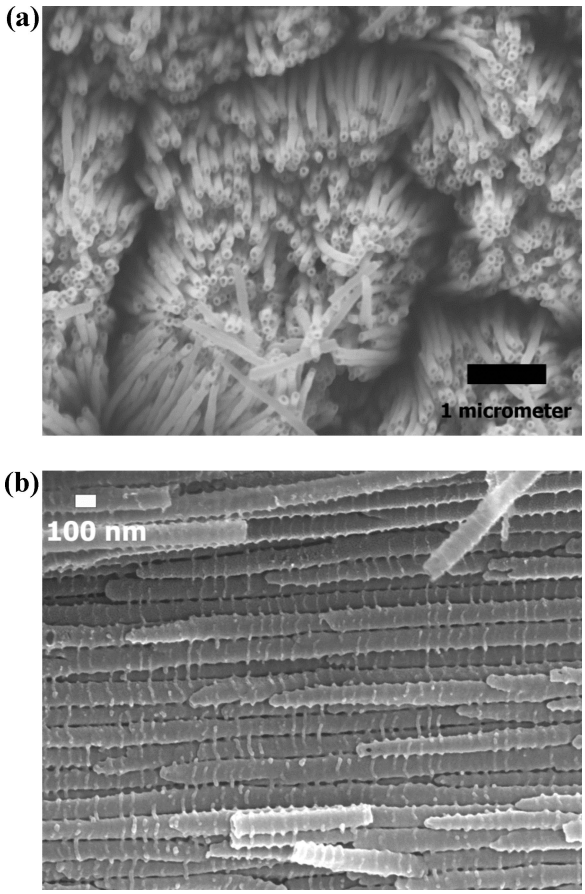

Figure 3. Field emission scanning electron microscope (FESEM) images of 14.4 μm TiO_2 nanotube array: (a) top view and (b) cross section.

circuit potential (V_{oc}) of 723 mV, and a fill-factor of 0.63 resulting in an overall conversion efficiency of 6.1%. Various TiO_2 nanotube array samples were sensitized with N-719 and Ru-TPA-NCS by immersing them overnight in their respective dye solutions. The dyes were then desorbed from their respective dye-coated electrodes into methanolic KOH containing 50 vol % *N*,*N*′-dimethylformamide (DMF). From the amount of desorbed dye, the surface coverage of dye was determined with the results shown in Table 2. The similar values of the surface coverage confirm that the increased optical density of the Ru-TPA-NCS coated samples arises from the higher extinction coefficient of the dye. Table 2 also indicates that the surface coverage of the dyes on 1 μm long transparent nanotube arrays is relatively poor, increasing by nearly a factor of 4 with the $TiCl_4$ treatment.

Frontside illumination was employed using 1 μm long transparent nanotube arrays on fluorine-doped tin oxide (FTO) coated glass. The details of the fabrication of transparent nanotubes have been explained elsewhere.[34] Briefly, 1 μm films of Ti were magnetron sputtered onto FTO coated glass substrates, which were subsequently anodized to form nanotubes. The crystallinity inducing anneal was performed at 450 °C to reduce the degradation in the resistivity of the FTO layer. The resulting nanotubes were 1 μm long with an average pore diameter of 100 nm. Unlike the nontransparent nanotubes which are anodized in formamide, transparent nanotubes were formed by anodizing them

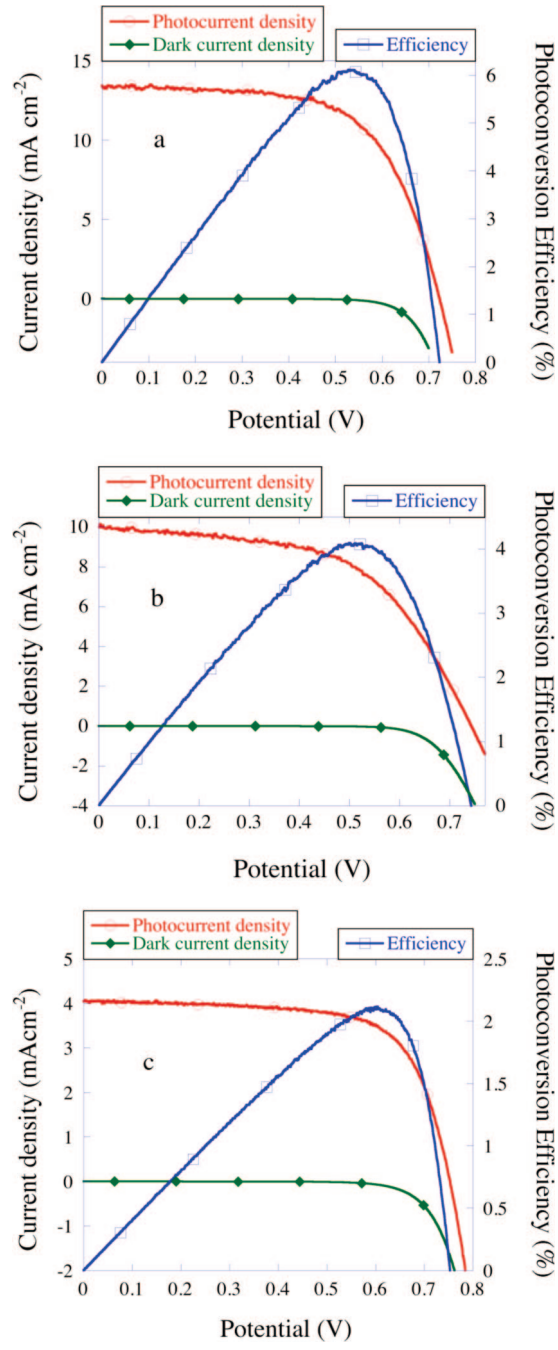

Figure 4. (a) Current−voltage characteristics of backside illuminated solar cells with Ru-TPA-NCS sensitized 14.4 μm long TiO_2 NT array under 1 sun AM 1.5 illumination. (b) Current−voltage characteristics of frontside illuminated solar cells with Ru-TPA-NCS sensitized 1 μm long $TiCl_4$ treated TiO_2 nanotube array under 1 sun AM 1.5 illumination. (c) AM 1.5 current−voltage characteristics of a $TiCl_4$-treated 1 μm long transparent nanotube array with N-719.

in an ethylene glycol based electrolyte which results in smoother nanotubes. Hence, the transparent nanotube array samples were subjected to a $TiCl_4$ treatment by placing them in a 0.05 M $TiCl_4$ solution for 30 min at 70 °C within airtight bottles. Subsequently, these samples were rinsed with water and ethanol and annealed in air at 450 °C for 30 min. We believe that the $TiCl_4$ treatment improves performance by increasing the effective surface area available for dye

Table 2. Surface Coverage on Nanotube Arrays of N-719 and Ru-TPA-NCS Determined by Dye Desorption

nanotube type	N-719 (nmol cm^{-2})	Ru-TPA-NCS (nmol cm^{-2})
14.4 μm nontransparent	181	189
1 μm transparent	3.68	5.76
1 μm transparent ($TiCl_4$ treated)	17.3	20.5

adsorption by increasing the roughness of the tube walls. Further, the $TiCl_4$ treatment appears to improve bonding between the TiO_2 and the dye, resulting in better charge injection.[35] The $TiCl_4$ treated transparent nanotube arrays were sensitized with Ru-TPA-NCS dye and used to fabricate solar cells, whose $I-V$ characteristics are shown in Figure 4b. With transparent nanotube arrays, the commercially available redox electrolyte MPN-100 (Solaronix, Inc., Switzerland) containing 100 mM of tri-iodide in methoxypropionitrile was used. A conductive glass slide sputter-coated with 80 nm of platinum was used as the counter-electrode for the transparent nanotube array-based solar cells, which were subjected to front-side illumination, where light is incident on the TiO_2 nanotube array after passing through the FTO coated glass. In Figure 4b, we see that a 1 μm long TiO_2 nanotube array yields a short circuit photocurrent density of 10.1 mA cm^{-2}, an open circuit potential of 743 mV, and a fill factor of 0.55 resulting in an overall conversion efficiency of 4.1%. In Figure 4c, we show the performance of a similar solar cell constructed by sensitizing a $TiCl_4$-treated 1 μm long transparent nanotube array with N-719. While the use of N-719 results in slightly larger values of the open circuit potential, the short circuit photocurrent density J_{sc} is nearly half that obtained with Ru-TPA-NCS sensitization because of the smaller amount of light harvested.

The action spectra of the transparent and nontransparent nanotube array-based solar cells are shown in Figure 5; overlap integrals of the solar cell AM 1.5 global solar irradiance action spectra provided a good match to the values of short circuit photocurrent shown in Figure 4. The inset of Figure 5 shows the effect of iodine concentration in the electrolyte on the transmittance of a blank solar cell constructed using a plain glass slide and another slide of FTO coated glass with redox electrolyte introduced between the clamped slides using the SX-1170 spacer. The extent of light absorption increases as a function of the iodine content in the redox electrolyte. For the frontside illuminated transparent nanotube array samples, photonic losses due to light absorption by the redox electrolyte are not experienced. Consequently, the incident monochromatic photon-to-electron conversion efficiency (IPCE) plots of the two solar cell geometries are significantly different. The backside illuminated solar cells constructed using a redox electrolyte containing 0.01 M I_2 exhibit their IPCE maximum at a wavelength of 563 nm while the frontside illuminated cells have their IPCE maximum at 433 nm. By considering that the transmittance through the blank backside illuminated solar cell is only 85% at the 563 nm, the Ru-TPA-NCS coated 14.4 μm long TiO_2 nanotube arrays achieve near quantitative conversion of incident photons into electrons.

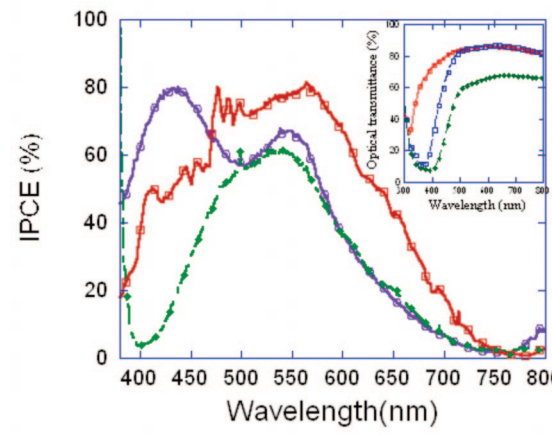

Figure 5. Photocurrent action spectra of Ru-TPA-NCS sensitized backside illuminated 14.4 μm TiO_2 nanotubes using 0.01 M I_2 containing redox electrolyte (—□—); using 0.1 M I_2 containing redox electrolyte (—○—); and frontside illuminated 1 μm long transparent TiO_2 NT (—◆—) solar cells. The inset shows the optical transmittance of blank solar cells with different concentrations of iodine in the redox electrolyte: 0.01 M (red), 0.02 M (blue), and 0.03 M (green).

Examination of the action spectrum of the frontside illuminated solar cell reveals how a 1 μm thick film of TiO_2 nanotube arrays is able to generate 10 mA cm^{-2} of photocurrent under AM 1.5 illumination. At 423 nm, close to the observed IPCE maximum for this solar cell, the molar extinction coefficient of Ru-TPA-NCS is a very high 54 500 M^{-1}, more than 5 times the value for N-719, thus enabling the achievement of ~80% conversion of incident photons at this wavelength into electrons.

To investigate the charge collection properties of the various dye coated solar cells, we employed open-circuit photovoltage decay (OCVD) measurements. The OCVD measurement consists of turning off the illumination at steady state and then monitoring the subsequent decay of the photovoltage V_{oc}.[36] In our case, we exposed the dye coated solar cells to AM 1.5 illumination for 100 s in a dark room before turning off the illumination. We measured the transient values of the open circuit potential as a function of time for 400 s after the illumination was turned off. For all OCVD measurements, we used the redox electrolyte MPN-100 containing 100 mM of tri-iodide. Assuming electron recombination occurs only with the electrolyte, the potential dependent electron lifetime $\tau_n(V_{oc})$ (really a response time) is given by the reciprocal of the derivative of the decay curve normalized by the thermal voltage:[36,37]

$$\tau_n = \frac{-k_B T}{e}\left(\frac{dV_{oc}}{dt}\right)^{-1} \quad (1)$$

Figure 6 shows the response times of various dye coated nanotube array-based solar cells. In addition, the response time plot of a dye sensitized nanocrystalline particulate electrode solar cell (pink curve), reconstructed from the data given in ref 36 is also displayed. The detailed $\tau_n(V_{oc})$ curves contain useful information regarding electronic recombination processes in the DSC. At high quasi-Fermi level E_F values (V_{oc} > 0.7 V), one observes the free conduction band electron

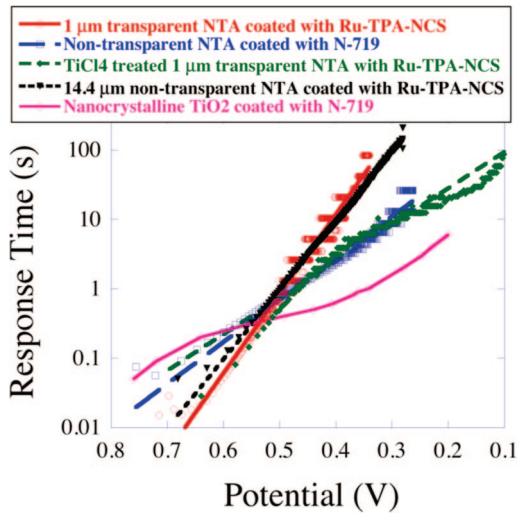

Figure 6. Response time determined from open circuit photovoltage decay measurements for various dye sensitized solar cells. All responses except that of the nanocrystalline TiO_2 are curve fit using an exponential line.

lifetime which is a constant given by τ_{cb}:[38]

$$\tau_{cb} = \frac{1}{e_{ox}^{(cb)}(E_c)} \tag{2}$$

The variable $e_{ox}^{(cb)}(E_c)$ denotes the conduction band transition probability, determined by the rate constant for isoenergetic electron transfer and the probability densities of the fluctuating energy levels in solution given by the Marcus−Gerischer model for electron transfer.[38]

For $E_F < 0.7$ eV, charge transfer is still dominated by conduction band states, but the bulk trap capacitance $C_\mu^{(traps)}$ becomes larger than the conduction band capacitance $C_\mu^{(cb)}$. In this case, the response time is given by:[38]

$$\tau_n = \frac{C_\mu^{(traps)}}{C_\mu^{(cb)}}\tau_{cb} \tag{3}$$

In this regime, expression 3 predicts a linear shape in the log/linear response time plot of Figure 6. In our experiments using TiO_2 nanotube arrays (NTAs), we observed that the V_{oc} values obtained with N-719 were consistently higher than those obtained with Ru-TPA-NCS by 5−10 mV. Whether this is intrinsic to the dye or a function of dye purity, dye−nanotube interaction, and so forth is not known at this point. Consequently, in the region of high V_{oc} values, the N-719 dye shows a higher recombination lifetime by the OCVD technique than Ru-TPA-NCS. For nanocrystalline electrodes, in the region of lower V_{oc} values, the linear dependence turns into a curved one since the charge transfer is now governed by the distribution of surface traps with a lifetime given by:[38]

$$\tau_n = \frac{C_\mu^{(traps)}}{C_\mu^{(st)} e_{ox}^{(st)}(E_F)}\tau_{cb} \tag{4}$$

where $C_\mu^{(st)}$ is the chemical capacitance of the surface traps and $e_{ox}^{(st)}$ is the transition probability for electron transfer from the semiconductor to the oxidized species in the liquid electrolyte.

For all nanotube array based solar cells, the response time plot remains linear with potential, implying that electron transfer through the conduction band states is dominant up to very low values of the Fermi level in the TiO_2 film. This suggests the nanotube array samples have a smaller number of surface traps compared with nanocrystalline electrodes or an exponential distribution of traps with a reduced depth.[38] We found that the values of the maximum open circuit photovoltage generated with the Ru-TPA-NCS dye are 50−100 mV smaller than that generated with N-719 dye. However, the slopes of the response time plot for the nanotube array cells (both transparent and nontransparent) sensitized with Ru-TPA-NCS are similar and significantly higher than that observed for N-719 sensitization.

Since all variables used in expressions 2 and 3 are dependent on electronic states within the nanotubular semiconductor, and as such are dye-independent, it appears that the transition probability for electron transfer from the Ru-TPA-NCS coated nanotubular TiO_2 to the electrolyte ionic species is lower than that for N-719. At first glance, this is somewhat counter-intuitive; since the size of the Ru-TPA-NCS molecule is larger than N-719, the self-assembled monolayer it forms on the TiO_2 surface would be expected to be less well-packed than N-179 because of the steric hindrance from the additional bulky triphenylamine groups. The resulting gaps in the Ru-TPA-NCS monolayer would provide less blocking behavior and allow easier access for the electrolyte ions to the TiO_2 surface. Yet, our work indicates the slope of the response time plot to be much higher for Ru-TPA-NCS with lifetimes approaching 100 s at low V_{oc} values. One possibility is that the Ru-TPA-NCS forms a more closely packed layer than N-719. Alternatively, we surmise that (a) even though the Ru-TPA-NCS layer is less closely packed, the nonpolar TPA end groups may provide similar or better blocking action against electrolyte ionic species, and (b) the consequent larger spatial separation between the TiO_2 surface and the electrolyte ions due the larger size of the donor antenna molecule results in a lower transition probability. Additionally, dipole effects at the interface caused by the donor antenna dye may also play a role here in determining the charge transfer and recombination dynamics. Figure 6 shows that with the $TiCl_4$ treatment the slope of the response time plot deviates from linearity with curvature increasing at lower V_{oc} values. Hence, with the $TiCl_4$ treatment, the recombination dynamics of the nanotube array appear to acquire more of a nanoparticulate character.

In summary, the much higher molar extinction coefficient of the donor antenna dye Ru-TPA-NCS allows a 1 μm thick film of dye sensitized nanotubular titania to achieve a conversion efficiency in excess of 4% in a liquid junction solar cell. By increasing the length of the transparent nanotube array electrodes into the tens of microns, a clear pathway toward the realization of very high efficiency dye sensitized solar cells using Ru-TPA-NCS is seen. The performance of backside illuminated solar cells is limited by light absorption losses resulting from the device geometry, yet photoconversion efficiencies of 6.1% and IPCE values

of up to 82% have been obtained because of maximal light harvesting with very high surface area long nanotube array electrodes sensitized with the highly absorbing donor antenna dye. It is known from previous work that the Ru-TPA-NCS dye provides improved performance in solid state solar cells, due partly to the improved wetting of the dye by the spiro-OMETAD hole transporting layer[24] and also to the increased spatial separation of the final charge separate states reducing the interfacial recombination losses.[22,23] Herein, we demonstrate that in liquid junction solar cells the donor antenna dye sensitized solar cells exhibit larger recombination lifetimes attributable to a combination of two factors: a reduced influence of surface trap states in nanotube array electrodes and a lower transition probability for back electron transfer from Ru-TPA-NCS coated TiO_2 to oxidized electrolyte species.

Acknowledgment. C.A.G. gratefully acknowledges support of this work by the Department of Energy under Grant DE-FG02-06ER15772. J.B. is grateful for an Alexander von Humboldt fellowship. M.T. acknowledges financial support for this work from SFB 481, German Research Council (DFG). The authors thank the referees for their helpful comments and suggestions.

Supporting Information Available: Assembly and testing details of solar cells fabricated using 14 μm long nontransparent nanotubes sensitized with Ru-TPA-NCS. This material is available free of charge via the Internet at http://pubs.acs.org.

References

(1) Yang, L. X.; Yang, W. Y.; Cai, Q. Y. *J. Phys. Chem. C* **2007**, *111*, 16613.
(2) Zhang, Z. H.; Yuan, Y.; Fang, Y. J.; Liang, L. H.; Ding, H. C.; Shi, G. Y.; Jin, L. T. *J. Electroanal. Chem.* **2007**, *610*, 179.
(3) Liu, Z.; Zhang, X.; Nishimoto, S.; Jin, M.; Tryk, D. A.; Murakami, T.; Fujishima, A. *J. Phys. Chem. C* **2008**, *112*, 253.
(4) Yang, L.; He, D.; Cai, Q.; Grimes, C. A. *J. Phys. Chem. C* **2007**, *111*, 8214.
(5) Mor, G. K.; Shankar, K.; Paulose, M.; Varghese, O. K.; Grimes, C. A. *Nano Lett.* **2005**, *5*, 191.
(6) Shankar, K.; Mor, G. K.; Prakasam, H. E.; Yoriya, S.; Paulose, M.; Varghese, O. K.; Grimes, C. A. *Nanotechnology* **2007**, 18, Article No. 065707.
(7) Mohapatra, S. K.; Misra, M. *J. Phys. Chem. C* **2007**, *111*, 11506.
(8) Mor, G. K.; Prakasam, H. E.; Varghese, O. K.; Shankar, K.; Grimes, C. A. *Nano Lett.* **2007**, *7*, 2356.
(9) Mor, G. K.; Shankar, K.; Paulose, M.; Varghese, O. K.; Grimes, C. A. *Nano Lett.* **2006**, *6*, 215.
(10) Mor, G. K.; Shankar, K.; Paulose, M.; Varghese, O. K.; Grimes, C. A. *Appl. Phys. Lett.* **2007**, 91 Art. No. 152111.
(11) Shankar, K.; Mor, G. K.; Prakasam, H. E.; Varghese, O. K.; Grimes, C. A. *Langmuir* **2007**, *23*, 12445.
(12) Varghese, O. K.; Gong, D. W.; Paulose, M.; Ong, K. G.; Dickey, E. C.; Grimes, C. A. *Adv. Mater.* **2003**, *15*, 624.
(13) Varghese, O. K.; Yang, X.; Kendig, J.; Paulose, M.; Zeng, K.; Palmer, C.; Ong, K. G.; Grimes, C. A. *Sensor Letters* **2006**, *4*, 120.
(14) Popat, K. C.; Eltgroth, M.; LaTempa, T. J.; Grimes, C. A.; Desai, T. A. *Biomaterials* **2007**, *28*, 4880.
(15) Popat, K. C.; Eltgroth, M.; La Tempa, T. J.; Grimes, C. A.; Desai, T. A. *Small* **2007**, *3*, 1878.
(16) Popat, K. C.; Leoni, L.; Grimes, C. A.; Desai, T. A. *Biomaterials* **2007**, *28*, 3188.
(17) Grimes, C. A. *J. Mater. Chem.* **2007**, *17*, 1451.
(18) Mor, G. K.; Varghese, O. K.; Paulose, M.; Shankar, K.; Grimes, C. A. *Solar Energy Materials and Solar Cells* **2006**, *90*, 2011.
(19) Ong, K. G.; Varghese, O. K.; Mor, G. K.; Shankar, K.; Grimes, C. A. *Solar Energy Materials and Solar Cells* **2007**, *91*, 250.
(20) Zhu, K.; Neale, N. R.; Miedaner, A.; Frank, A. J. *Nano Lett.* **2007**, *7*, 69.
(21) Karthikeyan, C. S.; Wietasch, H.; Thelakkat, M. *Adv. Mater.* **2007**, *19*, 1091.
(22) Handa, S.; Wietasch, H.; Thelakkat, M.; Durrant, J. R.; Haque, S. A. *Chem. Commun.* **2007**, 1725.
(23) Haque, S. A.; Handa, S.; Peter, K.; Palomares, E.; Thelakkat, M.; Durrant, J. R. *Angewandte Chemie-International Edition* **2005**, *44*, 5740.
(24) Karthikeyan, C. S.; Peter, K.; Wietasch, H.; Thelakkat, M. *Solar Energy Materials and Solar Cells* **2007**, *91*, 432.
(25) Nazeeruddin, M. K.; Kay, A.; Rodicio, I.; Humphrybaker, R.; Muller, E.; Liska, P.; Vlachopoulos, N.; Gratzel, M. *J. Am. Chem. Soc.* **1993**, *115*, 6382.
(26) Prakasam, H. E.; Shankar, K.; Paulose, M.; Varghese, O. K.; Grimes, C. A. *J. Phys. Chem. C* **2007**, *111*, 7235.
(27) Shankar, K.; Mor, G. K.; Fitzgerald, A.; Grimes, C. A. *J. Phys. Chem. C* **2007**, *111*, 21.
(28) Allam, N. K.; Grimes, C. A. *J. Phys. Chem. C* **2007**, *111*, 13028.
(29) Paulose, M.; Shankar, K.; Yoriya, S.; Prakasam, H. E.; Varghese, O. K.; Mor, G. K.; Latempa, T. A.; Fitzgerald, A.; Grimes, C. A. *J. Phys. Chem. B* **2006**, *110*, 16179.
(30) Xiao, P.; Garcia, B. B.; Guo, Q.; Liu, D. W.; Cao, G. Z. *Electrochem. Commun.* **2007**, *9*, 2441.
(31) Regonini, D.; Bowen, C. R.; Stevens, R.; Allsopp, D.; Jaroenworaluck, A. *Physica Status Solidi a-Applications and Materials Science* **2007**, *204*, 1814.
(32) Yin, Y. X.; Jin, Z. G.; Hou, F.; Wang, X. *J. Am. Ceram. Soc.* **2007**, *90*, 2384.
(33) Richter, C.; Wu, Z.; Panaitescu, E.; Willey, R. J.; Menon, L. *Adv. Mater.* **2007**, *19*, 946.
(34) Mor, G. K.; Varghese, O. K.; Paulose, M.; Grimes, C. A. *Adv. Func. Mater.* **2005**, *15*, 1291.
(35) Sommeling, P. M.; O'Regan, B. C.; Haswell, R. R.; Smit, H. J. P.; Bakker, N. J.; Smits, J. J. T.; Kroon, J. M.; van Roosmalen, J. A. M. *J. Phys. Chem. B* **2006**, *110*, 19191.
(36) Zaban, A.; Greenshtein, M.; Bisquert, J. *ChemPhysChem* **2003**, *4*, 859.
(37) Fabregat-Santiago, F.; Garcia-Canadas, J.; Palomares, E.; Clifford, J. N.; Haque, S. A.; Durrant, J. R.; Garcia-Belmonte, G.; Bisquert, J. *J. Appl. Phys.* **2004**, *96*, 6903.
(38) Bisquert, J.; Zaban, A.; Greenshtein, M.; Mora-Sero, I. *J. Am. Chem. Soc.* **2004**, *126*, 13550.

NL080421V